Journal of Hazardous Materials 169 (2009) 77–87

Contents lists available at ScienceDirect

Journal of Hazardous Materials

journal homepage: www.elsevier.com/locate/jhazmat

Biomolecule-controlled hydrothermal synthesis of C–N–S-tridoped TiO_2 nanocrystalline photocatalysts for NO removal under simulated solar light irradiation

Yawen Wang[a], Yu Huang[a], Wingkei Ho[b], Lizhi Zhang[a,*], Zhigang Zou[c], Shuncheng Lee[b]

[a] Key Laboratory of Pesticide and Chemical Biology of Ministry of Education, College of Chemistry, Central China Normal University, Wuhan 430079, People's Republic of China
[b] Department of Civil and Structural Engineering, Research Center for Environmental Technology and Management, The Hong Kong Polytechnic University, Hong Kong, People's Republic of China
[c] Ecomaterials and Renewable Energy Research Center (ERERC), Department of Physics, Nanjing University, Nanjing 210093, People's Republic of China

ARTICLE INFO

Article history:
Received 5 September 2008
Received in revised form 18 December 2008
Accepted 17 March 2009
Available online 26 March 2009

Keywords:
L-Cysteine
Doped TiO_2 nanocrystals
Photocatalysis
NO
Removal

ABSTRACT

In this study, C–N–S-tridoped titanium dioxide (TiO_2) nanocrystals were synthesized by using a facile hydrothermal method in the presence of a biomolecule L-cysteine. This biomolecule could not only serve as the common source for the carbon, sulfur and nitrogen tridoping, but also could control the final crystal phases and morphology. The resulting materials were characterized by X-ray diffraction (XRD), scanning electron microscopy (SEM), transmission electron microscopy (TEM), X-ray photoelectron spectroscopy (XPS), nitrogen adsorption and UV–vis diffuse reflectance spectroscopy. XPS analysis revealed that S was incorporated into the lattice of TiO_2 through substituting oxygen atoms, N might coexist in the forms of N–Ti–O and Ti–O–N in tridoped TiO_2 and most C could form a mixed layer of carbonate species deposited on the surface of TiO_2 nanoparticles. The photocatalytic activities of the samples were tested on the removal of NO at typical indoor air level in a flow system under simulated solar light irradiation. The tridoped TiO_2 samples showed much higher removal efficiency than commercial P25 and the undoped counterpart photocatalyst. The enhanced visible light photocatalytic activity of C–N–S-tridoped TiO_2 nanocrystals was explained on the basis of characterizations. The possible formation process of the monodispersed C–N–S-tridoped anatase TiO_2 nanocrystals was also proposed. This study provides a new method to prepare visible light active TiO_2 photocatalyst.

1. Introduction

Titanium dioxide (TiO_2) is the most widely used photocatalyst for solar energy conversion, air purification, and wastewater treatment [1]. However, anatase TiO_2 can only absorb UV light with wavelengths less than 388 nm, which is about 4% of the solar spectrum. This means most of solar energy in form of visible light cannot be utilized. Therefore, many attempts have been made to extend the absorption of TiO_2 to visible light region. For instance, doping with transition metals, such as Cr, Co, V, W and Fe, extends the spectral response of TiO_2 into the visible region and thus enhances its photocatalytic activity [2–5]. However, transition metal ion-doped TiO_2 suffers from some serious drawbacks, such as thermal instability and low quantum efficiency of the photoinduced charge carriers (electron–hole pairs) [6]. Recently, researchers turn to explore nonmetal-doped TiO_2 including carbon, nitrogen, phosphorus, sulfur, iodine and fluorine doped photocatalysts [7–12]. More recently, the simultaneous doping of two or three kinds of nonmetal atoms into TiO_2 has attracted considerable interest, since it could result in a higher photocatalytic activity and special characteristics compared with single element doping into TiO_2. For example, Li et al. found that N–F-codoped TiO_2 nanomaterials had a higher visible light photocatalytic activity than TiO_2 doped only with nitrogen or fluorine [13,14]. Cong et al. prepared C–N-codoped TiO_2 nanoparticles with visible light photocatalytic activity [15,16]. Sun et al. synthesized C–S-codoped TiO_2 by the hydrolysis of tetrabutyl titanate in a mixed aqueous solution containing thiourea and urea [17]. Zhou et al. reported C–N–S-tridoped titanium dioxide powders with enhanced daylight-induced photocatalytic activity. Their C–N–S-tridoped titanium dioxide photocatalyst was prepared by calcining the mixture of TiO_2 xerogel and thiourea at 500 °C for 3 h [18]. The doped ions depend, to some extent, on ion sources. Thus, the selection of ion sources is curial for the preparation of nonmetal-ion-doped photocatalysts with high activity. Thiourea and urea have often been used as nonmetal ion sources because they can supply sulfur, nitrogen, and carbon. For instance, thiourea

* Corresponding author. Tel.: +86 27 6786 7535; fax: +86 27 6786 7535.
E-mail address: zhanglz@mail.ccnu.edu.cn (L. Zhang).

0304-3894/$ – see front matter © 2009 Elsevier B.V. All rights reserved.
doi:10.1016/j.jhazmat.2009.03.071

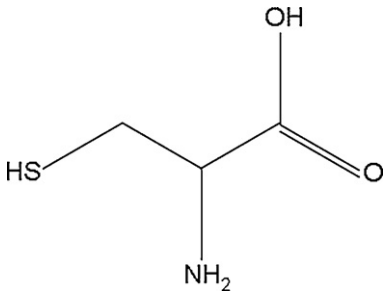

Fig. 1. Chemical structure of L-cysteine.

was used as sulfur [19] and nitrogen sources [20,21]. Urea was used as a nitrogen source [21,22]. While both thiourea and urea were used together as carbon sources [10].

A biomolecule is a molecule that naturally occurs in living organisms, including lipid, vitamin, amino acid, nucleotide, peptide, DNA, RNA, and so on [23]. Biomolecule consists primarily of carbon and hydrogen, along with nitrogen, oxygen, phosphorus and sulfur. Other elements sometimes are incorporated but are much less common. Recently, biomolecule-controlled/assisted synthesis methods have become a new and promising focus in the preparation of various nanomaterials due to their attracting structure and self-assembling role of biomolecules [24–26]. Interestingly, Komarneni and co-workers found that glutathione (GSH), a large polypeptide molecule, could be used as both the assembling molecule and the sulfur source to synthesize the highly ordered snowflake structure of bismuth sulfide nanorods under microwave irradiation [27]. Another biomolecule cysteine was often used as the sulfur source to prepare metal sulfides. For instance, Qian and coworkers synthesized antimony sulfide nanowires in the presence of cysteine [28]. Cysteine and glutathione were also used to prepare biostabilized CdS nanoparticles [29]. Zhang et al. synthesized the porous spongelike Ni_3S_2 nanostructures on Ni foil substrate with high electrochemical activity [30] and Bi_2S_3 flowerlike patterns with well-aligned nanorods in the presence of cysteine [31]. Tong and coworkers synthesized the ZnS nanostructured spheres using L-cysteine as the sulfur source [32].

In this study, we report a novel biomolecule-controlled hydrothermal method for the synthesis of C–N–S-tridoped TiO_2 nanocrystals. We chose a small peptide molecule L-cysteine as a common source of C, N, and S and interestingly find the addition of L-cysteine could control the final crystal phases and morphology. Fig. 1 is the chemical structure of L-cysteine [33]. In the cysteine molecule, there are three functional groups $–NH_2$, –COOH, and –SH, which all have a strong tendency to coordinate with inorganic cations [31]. Unlike the traditional nonmetal dopants like urea or thiourea, the amino group reacts with the carboxyl group of the neighboring cysteine molecule to form a dipeptide or polypeptide, which may play an important role in the growth of microstructures. We carefully characterized the resulting tridoped TiO_2 samples and tested their photocatalytic activities on the removal of the common indoor pollutant NO under simulated solar light irradiation.

2. Experimental section

2.1. Synthesis of C–N–S-tridoped TiO_2 nanocrystals

All of the chemicals were of commercially available analytical grade and used without further purification. In the typical procedure, 0.005 mol of $TiCl_4$ (98%) was slowly added into distilled water under magnetic stirring in an ice bath. During the addition, a large quantity of yellowish gas, presumably HCl, was released as a consequence of the hydrolysis of $TiCl_4$ in water. After stirring for several minutes, a transparent colorless solution was formed. Then, different amounts of L-cysteine were added to the solution under magnetic stirring. After the L-cysteine was dissolved completely, the resulting solution was placed in 20 mL Teflon-lined stainless-steel autoclaves. The autoclaves were maintained at 180 °C for 24 h and then air cooled to room temperature. The products were collected by centrifugation, thoroughly washed with ethanol and deionized water and dried in an oven at 50 °C. To control the phase of the samples and to compare the activity of the photocatalyst, we investigated the final morphologies of the samples as a function of molar ratios of L-cysteine to $TiCl_4$. During synthesis, we chose five different molar ratios of L-cysteine to $TiCl_4$, namely 0, 0.50, 1.00, 1.25 and 2.00, which were denoted as LT_0, $LT_{0.50}$, $LT_{1.00}$, $LT_{1.25}$ and $LT_{2.00}$, respectively.

2.2. Characterization

X-ray powder diffraction (XRD) patterns were obtained using a Philips MPD 18801 diffractometer using Cu-Kα radiation. X-ray photoelectron spectroscopy (XPS) measurements were performed on a PHI Quantum 2000 XPS System with a monochromatic Al Kα source and a charge neutralizer. All the binding energies were calibrated to the C1s peak at 284.8 eV of the surface adventitious carbon. Scanning electron microscopy (SEM) measurements were performed used a JSM-5600 SEM. Transmission electron microscopy (TEM) study was carried out on a Philips CM-120 electron microscopy instrument. The samples for TEM were prepared by dispersing the final powders in ethanol; the dispersion was then dropped on carbon–copper grids. High-resolution transmission electron microscopy (HRTEM) analysis was performed on a JEOL JSM-2010 microscope operating at 200 kV. The nitrogen adsorption and desorption isotherms at 77 K were measured using Micrometrics ASAP2010 system after samples were vacuum-degassed at 180 °C overnight. A Varian Cary 100 Scan UV–vis system equipped with a labsphere diffuse reflectance accessory was used to obtain the reflectance spectra of the catalysts over a range of 200–600 nm. Labsphere USRS-99-010 was employed as a reflectance standard.

2.3. Photocatalytic activity test

The photocatalytic activity experiments on the resulting samples for the oxidation of NO in air were performed at ambient temperature in a continuous flow reactor. The volume of the rectangular reactor which was made of stainless-steel and covered with Saint-Glass was 27.3 L (13 cm × 70 cm × 30 cm). Three sample dishes containing the photocatalysts powders were placed on a single path in the reactor. A 300 W commercial tungsten halogen lamp (General Electric) was used as the simulated solar light source. The lamp was vertically placed outside the reactor above the three sample dishes. Four mini fans were fixed around the lamp to avoid the temperature rise of the flow system. Furthermore, adequate distance was also kept from the lamp to the reactor for the same purpose to avoid temperature rise.

For activity test, an aqueous suspension of the photocatalyst sample was coated onto three dishes with a diameter of 5.0 cm. The weight of the photocatalyst used for each experiment was kept at 0.3 g. The dishes containing the photocatalyst were pretreated at 70 °C for several hours until a complete removal of water in the suspension and then cooled to room temperature before use.

The NO gas was photodegraded at ambient temperature. The NO gas was acquired from compressed gas cylinder at a concentration of 48 ppm NO (N_2 balance, BOC gas) with traceable National Institute of Stands and Technology (NIST) standard. The initial concentration of NO was diluted to about 400 ppb by the air stream supplied by a zero air generator (Thermo Environmental Inc. Model 111). The desired humidity level of the NO flow was controlled at

Table 1
Summary of physicochemical properties of the samples.

Sample	Contents of anatase (%)	Crystalline size of anatase (nm)	S_{BET} (m^2/g)	Average pore size of (nm)	Pore volume (cm^3/g)	Band gap (eV)	Degradation of NO after 25 min (%)
LT_0	41.1	12.7	58	12.1	0.17	2.95	0.1
$LT_{0.50}$	50.5	13.0	65	12.4	0.20	2.88	12
$LT_{1.00}$	92.6	11.8	97	12.1	0.29	2.84	17
$LT_{1.25}$	99.7	10.5	102	10.4	0.26	2.79	25
$LT_{2.00}$	100	9.3	99	10.1	0.25	2.71	13

70% (2100 ppmv) by passing the zero air streams through a humidification chamber. The gas streams were pre-mixed completely by a gas blender and the flow rate was controlled at 4 L min^{-1} by a mass flow controller. After the adsorption–desorption equilibrium among water vapor, gases and photocatalysts was achieved, the lamp was turned on. The concentration of NO was continuously measured by a chemiluminescence NO analyzer (Thermo Environmental Instruments Inc. Model 42c), which monitors NO, NO_2, and NO_x (NO_x represents NO + NO_2) with a sampling rate of 0.7 L min^{-1}. The conversion rate (%) of NO was defined according to the following equation:

$$\text{NOremoval}(\%) = \{([\text{NO}]\text{inlet} - [\text{NO}]\text{outlet})/[\text{NO}]\text{inlet}\} \times 100\%$$

Where $[NO]_{inlet}$ represents the concentration of NO in the feeding stream and $[NO]_{outlet}$ is the concentration of NO in the outlet stream. The reaction of NO with air was neglectable when performing a control experiment with or without light in the absence of photocatalyst.

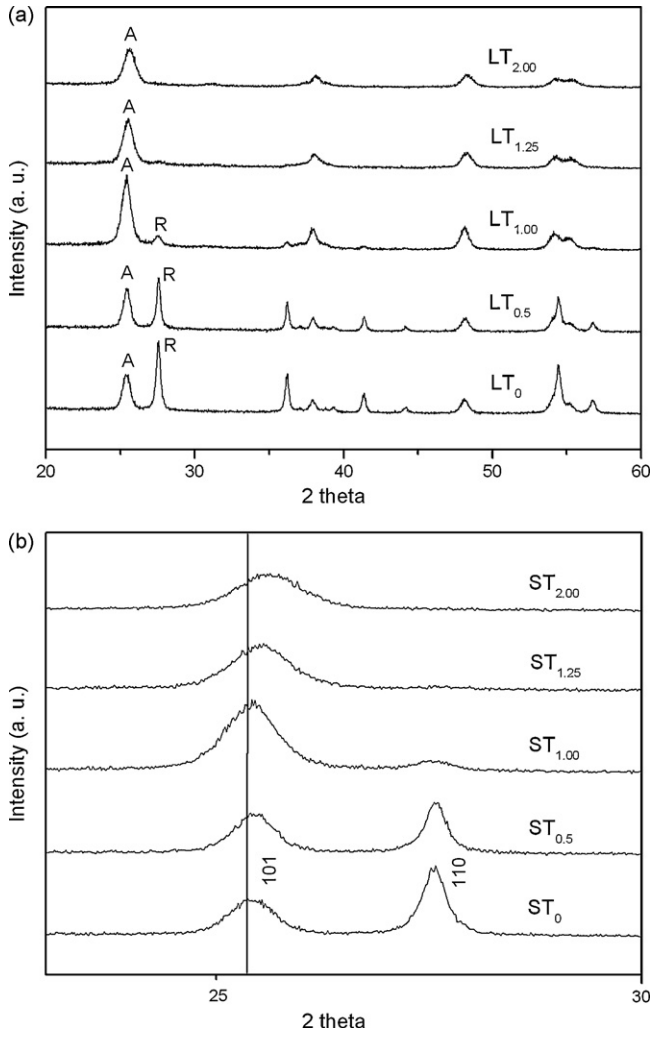

Fig. 2. XRD patterns of (a) pure TiO_2 and tridoped TiO_2 prepared by different molar ratio of L-cysteine to $TiCl_4$, and (b) the (1 0 1) plane of the samples.

3. Results and discussion

3.1. XRD patterns

Fig. 2a shows the XRD patterns of the as-prepared samples synthesized by the L-cysteine-assisted hydrothermal method at 180 °C. It is found that LT_0 contains both anatase (JCPDS file No. 21-1272) and rutile (JCPDS file No. 21-1276) with rutile phase in the majority according to their peak intensities. The anatase contents of the samples can be estimated from the respective XRD peak intensities according to the literature [34]. The contents of the anatase phases in the samples were summarized in Table 1. The anatase contents of the LT_0, $LT_{0.50}$, $LT_{1.00}$, $LT_{1.25}$ and $LT_{2.00}$ samples were found to be 41.1, 50.5, 92.6, 99.7, and 100 in percentage, respectively. It can be seen that with the increase of L-cysteine amount, the anatase content increased while the rutile content decreased. After the molar ratio of L-cysteine and Ti reached 1.25, only anatase was found in the resulting samples. This suggests that the addition of L-cysteine favors the formation of anatase and inhibits the formation of rutile. The XRD patterns of the (1 0 1) plane of the samples were shown in Fig. 2b. Compared to pure TiO_2 (LT_0), the peaks of the (1 0 1) plane of anatase of the doped TiO_2 shift slightly to higher values of 2θ. This shift suggests that the oxygen or Ti atoms in the lattice of anatase in doped samples may be substituted by other atoms. By applying the Scherrer formula on the anatase (1 0 1) diffraction peaks, the average crystallite sizes of the LT_0, $LT_{0.50}$, $LT_{1.00}$, $LT_{1.25}$ and $LT_{2.00}$ samples was found to be 13.0, 12.7, 11.8, 10.5 and 9.3 nm, respectively. Therefore, the addition of L-cysteine could slightly decrease average crystallite sizes of the samples.

3.2. XPS spectra

XPS was used to investigate chemical composition and the states of the elements in the as-prepared samples. The elemental compositions of all the resulting samples were summarized in Table 2. Undoped TiO_2 (LT_0) only contains C, O, and Ti elements, and the atomic composition of C, O, and Ti elements is 14.9, 57.9, and 27.2 at %, respectively. For the sample $LT_{1.25}$, C, O, Ti, N and S elements were detected (Fig. 3a). The atomic compositions of C, O, Ti, N, and S elements in sample $LT_{1.25}$ are 34.3, 47.5, 14.5, 2.1 and 1.6 at %, respectively. The C1s XPS spectra of sample $LT_{1.25}$ are shown in Fig. 3b. It can be fitted to three peaks at binding energies of 284.8, 286.6 and 288.4 eV. The first peak can be assigned to adventitious carbon adsorbed on the surface of the sample [35]. The other two peaks suggest the existence of C—O and C═O bonds of carbonate species [36]. The peak around 281 eV resulting from Ti–C bond was not observed [37]. Therefore, we conclude that the surface of doped TiO_2 sample is covered with carbonate species. This layer of carbonate species may inhibit the crystal growth as revealed by XRD results, and extend the absorption of TiO_2 to visible light [16].

Up to now, the assignment of the XPS peak of N1s has still been under debate. In many cases, the peak at about 396 eV is

Table 2
Summary of elemental composition of the samples.

Sample	Atomic composition (at %)				
	Ti	O	C	N	S
LT_0	27.2	57.9	14.9	–	–
$LT_{0.50}$	18.3	45.2	33.3	2.1	1.1
$LT_{1.00}$	16.9	46.1	33.7	1.9	1.4
$LT_{1.25}$	14.5	47.5	34.3	2.1	1.6
$LT_{2.00}$	10.2	51.2	32.8	1.8	4.0

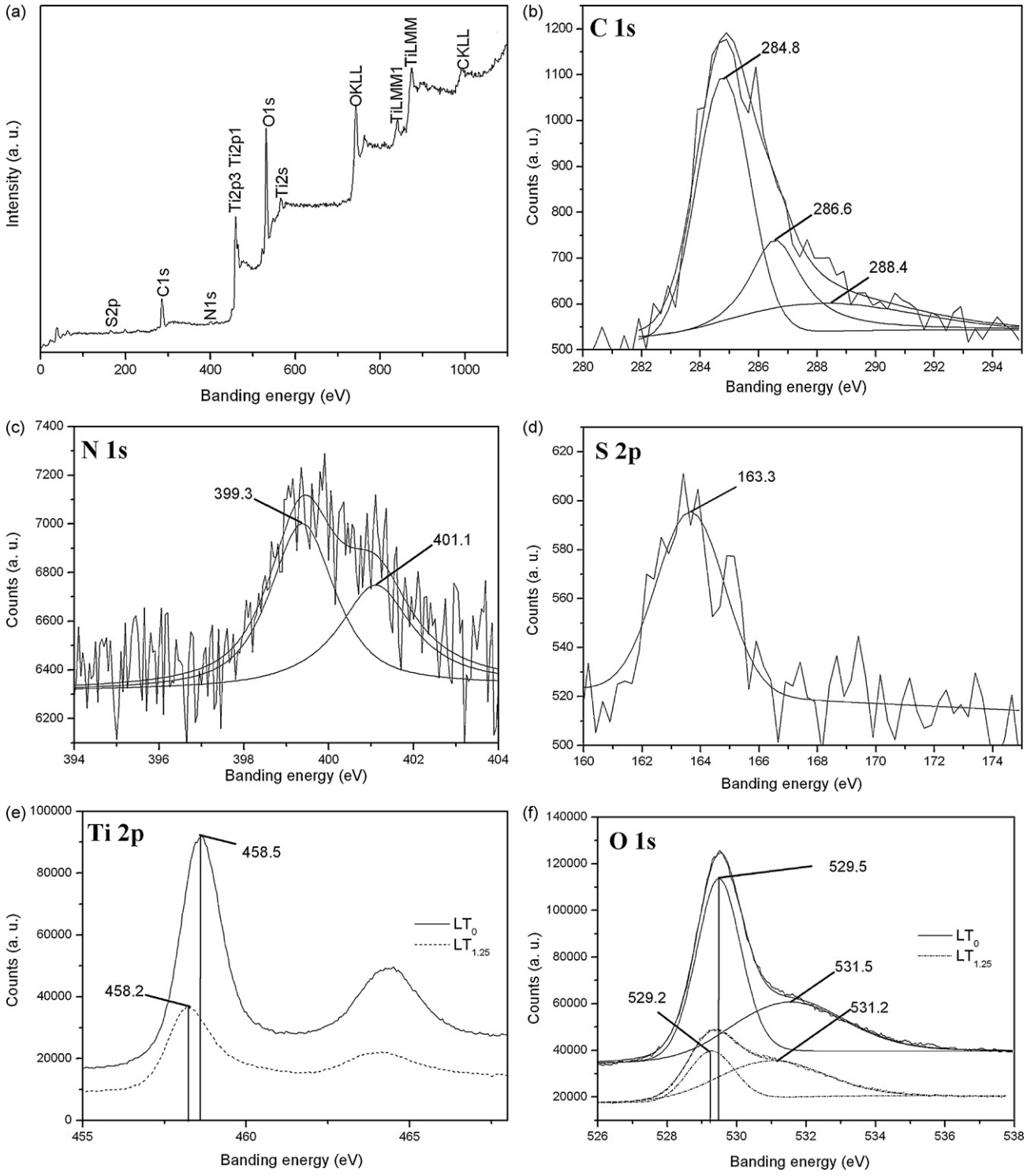

Fig. 3. Survey XPS (a), high-resolution spectra of C1s (b), N1s (c) and S2p (d) of the sample $LT_{1.25}$ and high-resolution spectra of Ti2p (e) and O1s (f) of the samples LT_0 and $LT_{1.25}$.

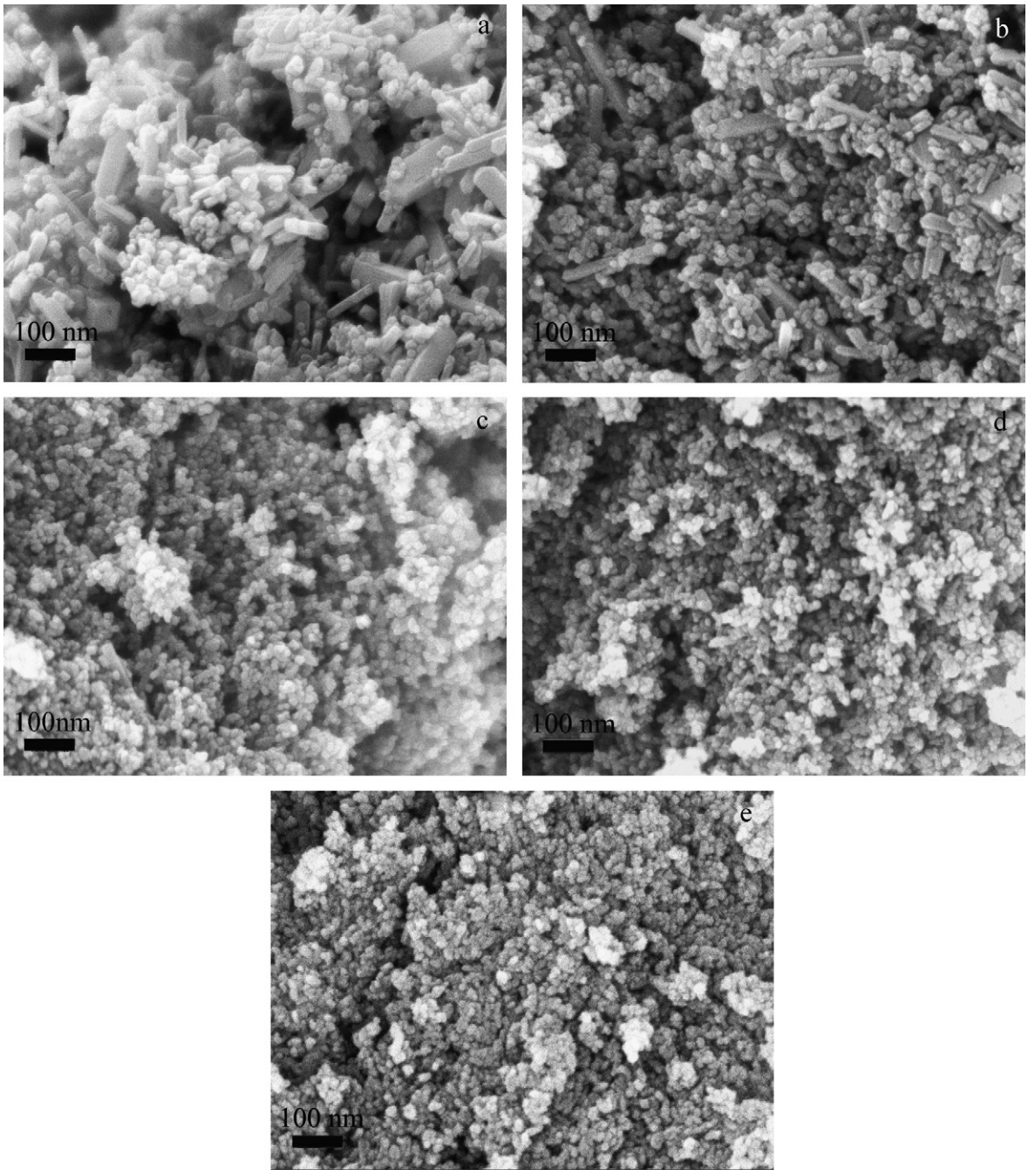

Fig. 4. SEM images of (a) LT_0, (b) $LT_{0.50}$, (c) $LT_{1.00}$, (d) $LT_{1.25}$, and (e) $LT_{2.00}$.

attributed to substitutional nitrogen doping [12]. In recent literature, the feature was found to be completely absent, while peaks at higher binding energies (399–404 eV) were detected [20,39]. In other cases, both features have been observed [13,14,12]. Fig. 3c shows the XPS spectra for the N1s region of the sample $LT_{1.25}$ and its fitting curves. It can be seen that there is a broad peak from 397 eV to 404 eV. After fitting, two peaks are obtained at 399.3 eV (peak 1) and 401.1 eV (peak 2), respectively. According to the literatures [12,38,39], the peak 1 can be attributed to the anionic N^- in the form of O–Ti–N. And the other peak 2 can be attributed to the presence of oxidized nitrogen such as Ti–O–N. Therefore, it can be concluded that two forms of N–Ti–O and Ti–O–N coexist in doped TiO_2.

Fig. 3d shows the high-resolution XPS spectrum of the S2p region of the sample $LT_{1.25}$. The sulfur atoms are in the state of S^{2-}, with a peak at about 163.3 eV, which corresponds to the anionic S^{2-} in Ti–S bond formed when some of the oxygen atoms in the TiO_2 lattice are replaced by sulfur atoms, [40] and no peaks are found around 169, 168 and 166 eV, which corresponds to the S^{6+}, S^{4+} and S^{2+} species, respectively. Umebayashi et al. [41] used theoretical calculations to depict the band gap narrowing when oxygen was replaced by sulfur in anatase TiO_2. They found that the sulfur dopant was in the anionic form when TiS_2 was used as the starting material. Similarly, in our case most of the sulfur in L-cysteine was decomposed and the residual sulfur would naturally remain as S^{2-} dopant to replace some of the oxygen atoms in the TiO_2 lattice during the hydrothermal process.

The XPS spectrum of $Ti2p_{3/2}$ in the sample $LT_{1.25}$ can be fitted as one peak at 458.2 eV which shows a red shift of 0.3 eV compared to the binding energy of Ti^{4+} in pure TiO_2 (Fig. 3e). Lower binding

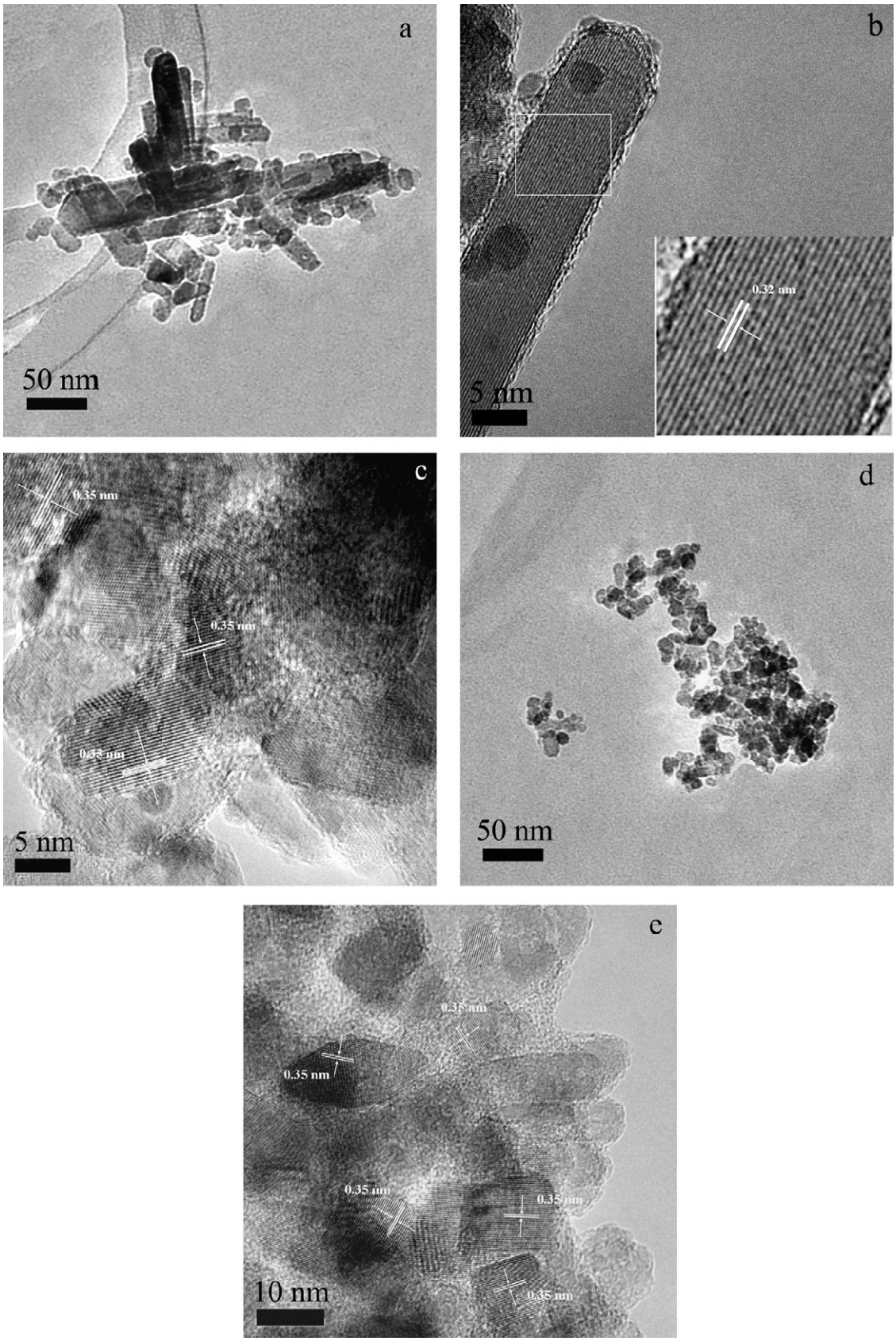

Fig. 5. TEM (a) and HRTEM (b, c) images of LT_0; and TEM (d) and HRTEM (e) images of $LT_{1.25}$.

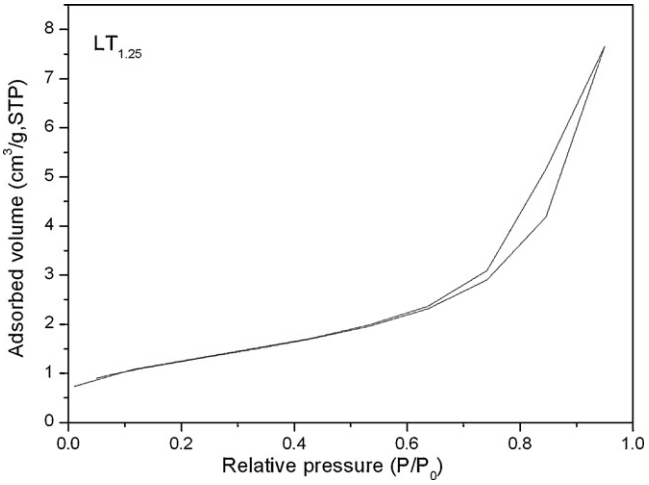

Fig. 6. Nitrogen adsorption–desorption isothermof the sample $LT_{1.25}$.

energy of Ti2p in doped TiO_2 suggests different electronic interactions of Ti with anions, which causes partial electron transformation and an increase of the electron density on Ti [38,42]. This further justifies that sulfur and nitrogen incorporate into the lattice and substitutes for oxygen [42].

Fig. 3f shows the high-resolution XPS spectrum of the O1s region of the samples $LT_{1.25}$ and LT_0. For the undoped TiO_2 (LT_0), the O1s peak comprises of a dominant peak at about 529.5 eV and a shoulder peak at about 531.5 eV. The lower energy peak is due to Ti–O bonding in TiO_2 and the higher energy peak is may be due to the C—O, C—O—O, and O—H bonds on the surface [43]. The O1s peak of the doped TiO_2 ($LT_{1.25}$) also consists of two peaks. The peak at 529.2 eV corresponds to the anionic O^{2-} in Ti–O bond in TiO_2. As for another peak at 531.2, Saha et al. [44] and Gyorgy et al. [45] attributed it to the presence of Ti—O—N bonds in N-doped TiO_2. Therefore, considering the presence of Ti—O—N bond according to the analysis of high-resolution XPS spectrum of the N1s region of the sample $LT_{1.25}$, we attributed the peak at 531.2 not only to C—O, C—O—O and O—H bonds but also to Ti—O—N bonds. The binding energy values of the O in the $LT_{1.25}$ shifted negatively by 0.3 compared to those in the undoped TiO_2 (LT_0), further confirming that N and S atoms substitute the O in the lattice of TiO_2. After the substitution, partial electrons would transfer from the N and S to the Ti and further to the O atom because of the higher electronegativity of oxygen than that of nitrogen and sulfur. This makes the N and S electron-deficient and the O electron-enriched, respectively. This substitution was confirmed by the peaks of the (1 0 1) surface of C, N, S-doped TiO_2 shift slightly to higher values of 2θ compared to undoped TiO_2 in XRD results.

3.3. SEM images

The SEM images of both doped and undoped samples are shown in Fig. 4. The undoped TiO_2 (LT_0) consisted of both nanorods and nanoparticles. The nanorods are 25–200 in length and 10–50 nm in diameter, while the nanoparticles are of uniform size of about 13 nm (Fig. 4a). With the addition of L-cysteine, the nanorods in the resulting doped samples became less and less and nanoparticles became more and more (Fig. 4b and c). When the molar ratio of L-cysteine to Ti was up to 1.25, the resulting samples were only composed of monodispersed nanoparticles as shown in Fig. 4d and e. After combining the XRD results and the SEM observations, we speculate that the nanorods and the nanopartilcles may be rutile and anatase, respectively. The appropriate addition of L-cysteine could produce monodispersed nanocrystals of C–N–S-tridoped TiO_2.

3.4. TEM images

The size, morphology and crystallinity of the products were further analyzed by TEM measurements. Fig. 5a shows the nanorods in LT_0 have widths of 10–50 nm and lengths of 25–200 nm and the sizes of nanoparticles are about 13 nm. The single-crystal nature of the nanorods in LT_0 was revealed by HRTEM (Fig. 5b). The lattice spacing is about 0.32 nm between adjacent lattice planes of the nanorods, corresponding to the distance between (1 1 0) crystal planes of the rutile phase. Fig. 5c reveals that nanoparticles in LT_0 are also single crystalline. For the nanoparticles, the lattice spacing of about 0.35 nm matches well with the distance between the (1 0 1) crystal planes of anatase TiO_2. Fig. 5d shows a representative TEM image of tridoped TiO_2 $LT_{1.25}$, which only contains nanoparticles of about 10 nm. The HRTEM image of the tridoped TiO_2 nanoparticles (Fig. 5e) displays the lattice spacing of the (1 0 1) plane of anatase (0.35 nm). Therefore, HRTEM analysis confirms our speculation that the nanorods and the nanopartilcles in the undoped and doped TiO_2 are rutile and anatase, respectively.

3.5. Nitrogen adsorption

The microstructures of the resulting samples were studied by nitrogen adsorption. Fig. 6 presents the nitrogen adsorption–desorption isotherms of the sample $LT_{1.25}$. It can be seen that the adsorption–desorption isotherms belong to type IV with an H3 type

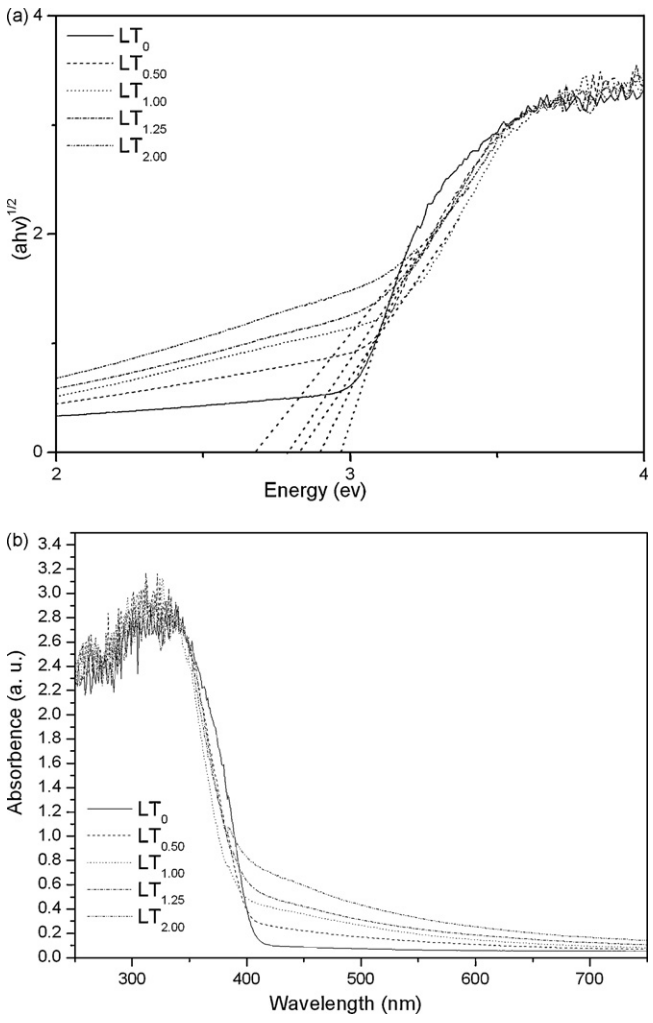

Fig. 7. Plots of the $(\alpha hv)^{1/2}$ versus the energy of absorbed light (a) and UV–vis diffuse reflectance spectra of the samples (b).

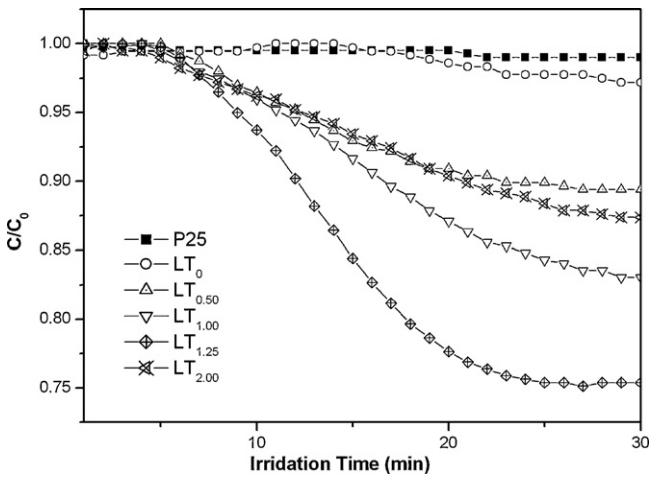

Fig. 8. Photocatalytic activities of the samples on the oxidation of NO. Residence time 3.72 min, humidity levels 2200 ppmv, 400 ppb NO.

hysteresis loop [46], which indicated the existence of mesopores in the resulting materials. The other samples LT_0, $LT_{0.50}$, $LT_{1.00}$, and $LT_{2.00}$ have the similar type nitrogen adsorption-desorption isotherms with that of $LT_{1.25}$. Table 1 summarizes the surface areas (S_{BET}), pore volumes (Vp), and pore diameters (dp) of different samples calculated by the BJH method based on the N_2 adsorption–desorption isotherms. From Table 1 we can see that the BET surface area and pore volume of the tridoped TiO_2 increased with the increase of L-cysteine amount. However, when the molar ratio of L-cysteine and Ti was up to 1.00, the BET surface areas and pore volumes of the tridoped TiO_2 did not change much. The average pore sizes of the samples decreased with the addition of L-cysteine.

3.6. Diffuse reflectance UV–vis spectroscopy

Fig. 7 displays UV–vis diffuse reflectance spectra of the resulting samples. As TiO_2 is an indirect transition semiconductor, plots of the $(\alpha hv)^{1/2}$ versus the energy of absorbed light afford the band gaps of the samples (as shown in Fig. 7a) The band gaps optically obtained in such a way were approximately 2.95, 2.88, 2.84, 2.79 and 2.71 eV for the sample LT_0, $LT_{0.50}$, $LT_{1.00}$, $LT_{1.25}$ and $LT_{2.00}$, respectively. It is apparent that the diffuse reflectance spectra of all the samples tridoped with carbon, nitrogen, and sulfur possess a red shift and their absorbance increase in the visible range from 400 nm to 600 nm. With the increasing of doping concentration, the visible light absorbance increases (Fig. 7b).

3.7. Photocatalytic NO removal

The indoor air quality (IAQ) has attracted more and more attentions in recent years. Nitrogen oxide is one of the most common gaseous pollutants found in the indoor environment with the concentration in the range of 70–500 parts-per-billion (ppb) levels. Photocatalysis technique provides a very promising solution for the removal of indoor air pollutants at low concentration. Fig. 8 shows the NO concentration changes versus irradiation time in the presence of the samples LT_0, $LT_{0.50}$, $LT_{1.00}$, $LT_{1.25}$, $LT_{2.00}$, and P25 under simulated solar light irradiation. Degussa P25 is a commercially available titania with mean particle size about 20–30 nm, Which contains 70 wt% anatase and 30 wt% rutile. P25 is widely studied and well known to have good photocatalytic activity [47]. Prior to the simulated solar light irradiation, the adsorption/desorption equilibrium between the gas and photocatalysts was reached. When the lamp was turned on, the photocatalytic reaction of NO on the photocatalysts was initiated. It was found that both the photolysis of NO in the absence of photocatalysts and its photooxidation in the presence of P25 were negligible under simulated solar light irradiation. After 30 min of degradation under simulated solar light irradiation, 0.1, 12, 17, 25 and 13% of NO were photocatalytically oxidized on the samples of LT_0, $LT_{0.50}$, $LT_{1.00}$, $LT_{1.25}$ and $LT_{2.00}$ respectively. Obviously, the photocatalytic activity of C–N–S-tridoped TiO_2 was much superior to that of P25 and undoped TiO_2 on the degradation of NO. With increasing doping amount, the photocatalytic activity of tridoped TiO_2 first increased and then decreased. The sample $LT_{1.25}$ possessed the highest activity to remove NO under simulated solar light irradiation. For the sample $LT_{1.25}$, the NO concentration at outlet gradually decreased to the lowest value after being irradiated for 27 min, and then kept almost unchanged,

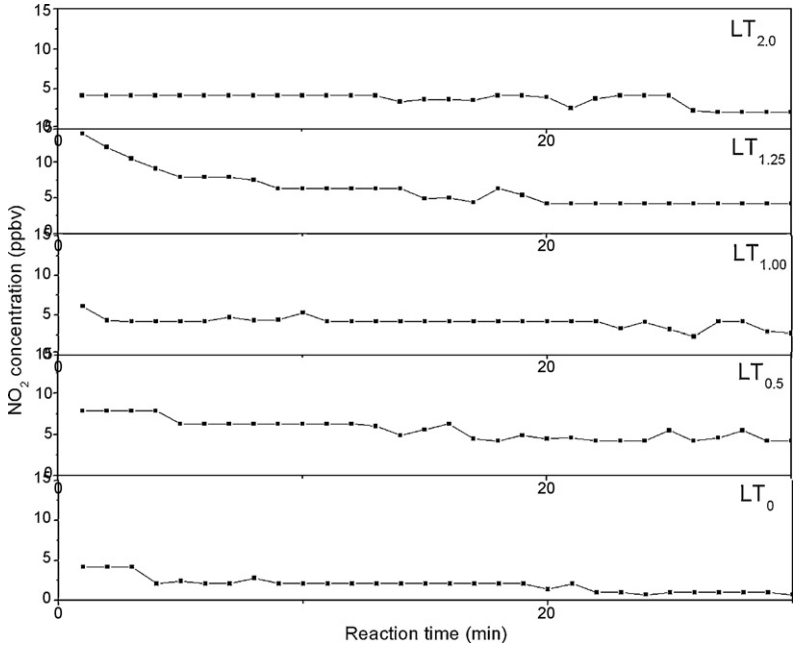

Fig. 9. NO_2 concentration of samples in outlet gas versus reaction time under simulated solar light irradiation.

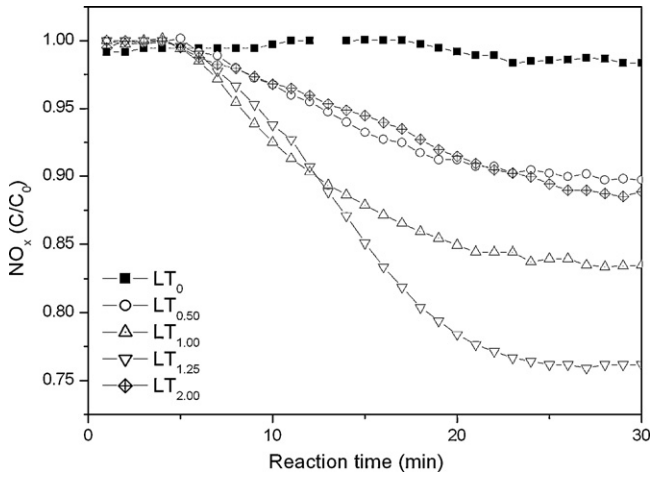

Fig. 10. Photocatalytic activities of the samples on the oxidation of NO_x. Residence time 3.72 min, humidity levels 2200 ppmv, 400 ppb NO.

indicating high stability and long-term activity of C–N–S-tridoped TiO_2 photocatalyst.

During the photoreaction, NO_2 was continuously formed and eventually transferred into HNO_3 in this photocatalytic oxidation environment. The NO_2 concentration of the samples in outlet gas was maintained 5–10 ppb which is at a very low level (Fig. 9). The conversion of NO_x for the catalysts of LT_0, $LT_{0.50}$, $LT_{1.00}$, $LT_{1.25}$ and $LT_{2.00}$ after 30 min simulated solar light irradiation was found to be 0.1, 10, 16, 24 and 11%, respectively (Fig. 10), similar to that of NO (Fig. 8).

It is known that photocatalytic process mainly takes place on the surface of catalysts and involves comprehensive competing reactions. Therefore, surface properties of TiO_2, such as surface acidity, defects, and hydroxyl groups can greatly affect its photocatalytic activity [48]. In our experiment, the oxidation reaction of NO was believed to be initiated by •OH radicals. In the presence of O_2, the OH radicals are formed as follows [49].

$$TiO_2 + h\nu \leftrightarrow h^+_{VB} + e^-_{CB} \quad (1)$$

$$e^-_{CB} + O_2 \rightarrow O_2^- \quad (2)$$

$$O_2^- + 2H^+ + e^-_{CB} \rightarrow H_2O_2 \quad (3)$$

$$H_2O_2 + O_2^- \rightarrow {}^\bullet OH + OH^- + O_2 \quad (4)$$

$$h^+ + H_2O \rightarrow {}^\bullet OH + H^+ \quad (5)$$

According to the above reactions, several reasons may account for the higher photoactivities of the C–N–S-tridoped TiO_2 under simulated solar light irradiation compared to P25 and the undoped TiO_2. One possible reason may be that the addition of L-cysteine could attribute to the transformation of rutile to anatase in TiO_2, and it is reported that anatase have the higher photocatalytic activities than rutile [50,51]. However, a recent study revealed the anatase/rutile mixed phase showed synergistic effect in enhancing the photocatalytic activity [52]. Hence, the difference of the

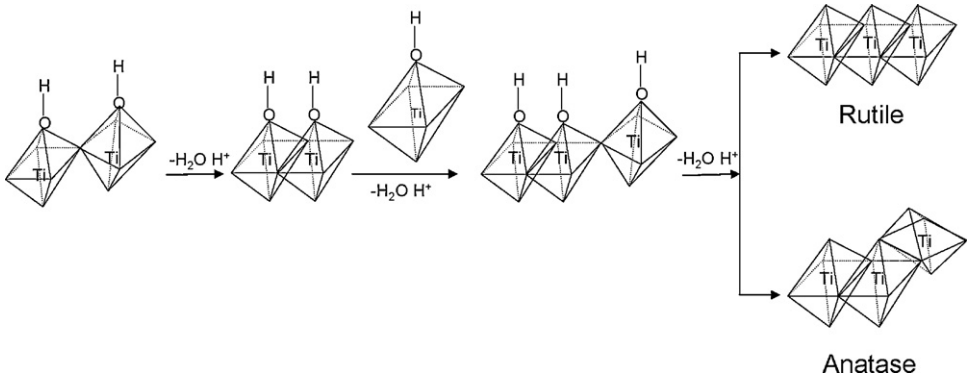

Scheme 1. Illustration of the possible formation mechanism of rutile and anatase TiO_2 under acid condition in the absence of L-cysteine.

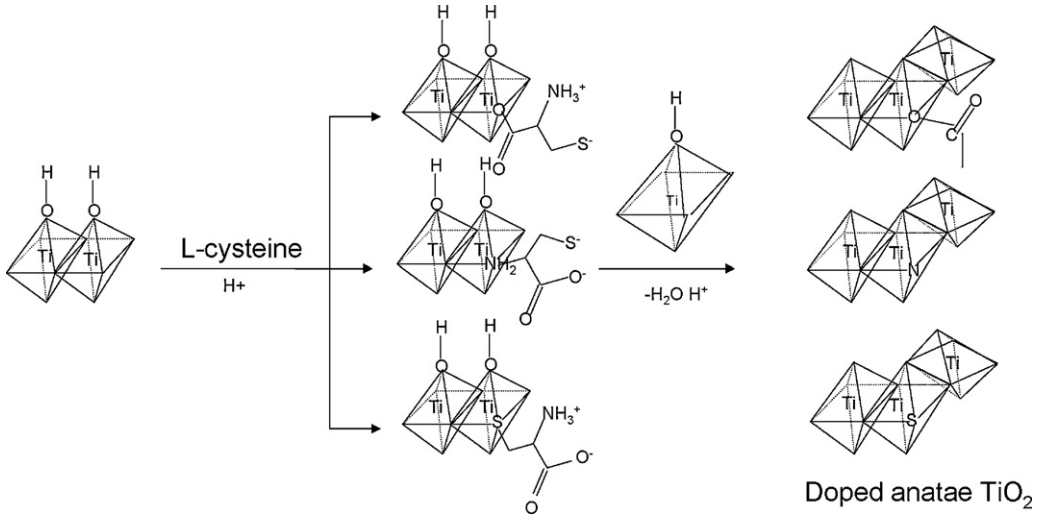

Scheme 2. Illustration of the possible formation mechanism of C–N–S-tridoped monodispersed anatase TiO_2 in the presence of L-cysteine.

anatase content should not be the main factor for the photocatalytic activity enhancement. The second possible reason may be the high surface area of the tridoped TiO_2, which was favorable for the adsorption of NO molecules. It has been reported that electron–hole recombination on the particle surface would be enhanced with increasing surface area [53]. The BET surface areas of all samples are shown in Table 1. Considering the surface area values of $LT_{1.00}$, $LT_{1.25}$ and $LT_{2.00}$ were very close, but the activity of the $LT_{1.25}$ sample was significantly higher than those of $LT_{1.00}$ and $LT_{2.00}$, we believe the photocatalytic activity enhancement by tridoping could not be attributed to that the larger surface area. Therefore, the visible light absorption and band gap narrowing should be the most important factors for the photocatalytic activity enhancement. It is generally accepted that carbon, nitrogen and sulfur doping can form a new states lie just above the valence band, which all could decrease the band gap of TiO_2 and absorb the visible light [11,39,40]. In this study, C–N–S tridoping could obviously extend the absorbance response range of TiO_2 into the visible region. This could strongly increase the number of photo-generated electrons and holes to participate in the photocatalytic reaction under simulated solar light irradiation with visible light in the majority. From Table 1, the activity changes of the C–N–S-tridoped TiO_2 are basically in accord with those of the band gaps of the samples. Therefore, we conclude that the photocatalytic activity enhancement is attributed to the visible light absorption and band gap narrowing resulted from tridoping and the C–N–S-tridoped TiO_2 is a promising visible light photocatalyst. The sample $LT_{1.25}$ possesses the maximum photocatalytic activity, suggesting that there is an optimum value for the doping. This phenomenon is reasonable, because too much dopant (like $LT_{2.00}$) would decrease the distance between trapping sites in a photocatalyst particle, which will increase the recombination rate to decrease the photocatalytic activity [54].

3.8. Possible formation processes of C–N–S-tridoped TiO_2 nanocrystals

It is known that the presence of H^+ or H_3O^+ catalyzes the dehydration of surface OH groups of neighboring octahedrons that share only one common vertex, thus linking them by sharing one edge (Scheme 1). When the two octahedrons sharing one edge is attacked by another TiO_6 octahedra complex, this H^+ or H_3O^+ catalyzing dehydration process occurs again, and there are two connecting possibilities among the TiO_6 octahedrons: one is the formation of linear chains of octahedrons by continuously sharing the opposite edge, which leads to the formation of rutile titania; the other is the formation of spinal or zigzag chains of octahedrons, which favors the formation of anatase or brookite [55,56]. Under acid conditions the hydroxide groups in neighboring octahedrons sharing one edge are protonated, the electrostatic repulsion between the neighboring octahedrons is prone to further share the opposite edge between neighboring octahedrons. Having thus aligned octahedrons by sharing the opposite edge between neighboring octahedrons, and with the adjacent linear chains of TiO_6 octahedrons sharing a pair of opposite edges further dehydrated and linked by shared vertexes to form a 3D structure, the formation of rutile will be favorable [55]. In our synthesis, the hydrolysis of $TiCl_4$ produced large amount of H^+ and led to high acidity of the solution. This high acidity would produce large amount of rutile TiO_2 nanorods in the undoped sample LT_0. If L-cysteine is present in the solution, all the three of groups $-NH_2$, –COOH, and –SH in L-cysteine are able to coordinate with the Ti atoms (Scheme 2) to bond the molecule of L-cysteine to the protonated neighboring octahedrons sharing one edge. When another TiO_6 octahedra complex attack the two octahedrons sharing one edge with the L-cysteine molecule bonding, only a spinal chain of octahedrons could form because of steric hindrance given by the L-cysteine molecules tightly linked to terminal Ti ions, and which would inhibit the formation of rutile TiO_2. Moreover, it is possible that the amino group reacts with the carboxyl group of the neighboring cysteine molecule to form a dipeptide or polypeptide that can serve as the bigger hindrance to the formation of rutile. Therefore, the addition of L-cysteine could inhibit the formation of rutile TiO_2 nanorods and favor the generation of monodispersed anatase nanocrystals tridoped with C, N, and S under hydrothermal treatment.

4. Conclusions

In summary, C–N–S-tridoped TiO_2 nanocrystals were prepared by a facile biomolecule-controlled hydrothermal method in the presence of L-cysteine. The biomolecule L-cysteine could not only serve as the common source of carbon, nitrogen and sulfur, but also control the final crystal phases and morphology. The resulting C–N–S-tridoped TiO_2 nanocrystals possessed much higher photocatalytic activity than the commercial P25 and the undoped counterpart photocatalyst on the removal of the common indoor pollutant NO under simulated solar light irradiation. The enhanced photocatalytic activity of tridoped TiO_2 nanocrystals was mainly attributed to the visible light absorbance and band gap narrowing of TiO_2 resulted from C–N–S-tridoping. This study provides a new way to prepare TiO_2 photocatalysts effectively working under solar light.

Acknowledgments

This work was supported by National Basic Research Program of China (973 program) (grant 2007CB613301), National Science Foundation of China (grants 20503009, and 20777026), program for New Century Excellent Talents in University (Grant NCET-07-0352), the Key Project of Ministry of Education of China (Grant 108097), and the Scientific Research Foundation for the Returned Overseas Chinese Scholars, State Education Ministry.

References

[1] M.R. Hoffmann, S.T. Martin, W. Choi, D.W. Bahnemann, Chem. Rev. 95 (1995) 69.
[2] E. Borgarello, J. Kiwi, M. Gratzel, E. Pelizzetti, M. Visca, J. Am. Chem. Soc. 104 (1982) 2996.
[3] M. Iwasaki, M. Hara, H. Kawada, H. Tada, S. Ito, J. Colloid Interface Sci. 224 (2000) 202.
[4] S. Klosek, D. Raftery, J. Phys. Chem. B 105 (2001) 2815.
[5] J. Zhu, F. Chen, J. Zhang, H. Chen, M. Anpo, J. Photochem. Photobiol. A 180 (2006) 196.
[6] W. Choi, A. Termin, M.R. Hoffmann, J. Phys. Chem. B 98 (1994) 13669.
[7] H. Irie, Y. Watanabe, K. Hashimoto, Chem. Lett. 32 (2003) 772.
[8] Y. Kuroda, T. Mori, K. Yagi, N. Makihata, Y. Kawahara, M. Nagao, S. Kittaka, Langmuir 21 (2005) 8026.
[9] S.U.M. Khan, M. Al-Shahry, W.B. Ingler Jr., Science 297 (2002) 2243.
[10] T. Ohno, T. Tsubota, K. Nishijima, Z. Miyamoto, Chem. Lett. 33 (2004) 2.
[11] W.J. Ren, Z.H. Ai, F.L. Jia, L.Z. Zhang, X.X. Fan, Z.G. Zou, Appl. Catal. B: Environ. 69 (2007) 138.
[12] R. Asahi, T. Morikawa, T. Ohwaki, A. Aoki, Y. Taga, Science 293 (2001) 269.
[13] D. Li, H. Haneda, S. Hishita, N. Ohashi, Chem. Mater. 17 (2005) 2588.
[14] D. Li, H. Haneda, S. Hishita, N. Ohashi, Chem. Mater. 17 (2005) 2596.
[15] Y. Cong, F. Chen, J. Zhang, M. Anpo, Chem. Lett. 35 (2006) 800.
[16] D. Chen, Z.Y. Jiang, J.Q. Geng, Q. Wang, D. Yang, Ind. Eng. Chem. Res. 46 (2007) 2741.
[17] H.Q. Sun, Y. Bai, Y.P. Cheng, W.Q. Jin, N.P. Xu, Ind. Eng. Chem. Res. 45 (2006) 4971.
[18] M.H. Zhou, J.G. Yu, J. Hazard. Mater. 7 (2007) 113.
[19] C. Lettmann, K. Hildenbrand, H. Kisch, W. Macyk, W.F. Maier, Appl. Catal. B: Environ. 32 (2001) 215.
[20] S. Sakthivel, M. Janczarek, H. Kisch, J. Phys. Chem. B 108 (2004) 19384.
[21] R. Bacsa, J. Kiwi, T. Ohno, P. Albers, V. Nadtochenko, J. Phys. Chem. B 109 (2005) 5994.
[22] K. Kobayakawa, Y. Murakami, Y. Sato, J. Photochem. Photobiol. A: Chem. 170 (2005) 177.
[23] Oxford Dictionary of Biochemistry and Molecular Biology, Oxford University Press, 2006, p. 76.
[24] T. Douglas, E. Strable, D. Willits, A. Aitouchen, M. Libera, M. Young, Adv. Mater. 14 (2002) 415.

[25] T. Douglas, D.P.E. Dichson, S. Betteridge, J. Charnoch, C.D. Garner, S. Mann, Science 269 (1995) 54.
[26] A. Ahmad, P. Mukherjee, D. Mandal, S. Senapati, M.I. Khan, R. Kumar, M. Sastry, J. Am. Chem. Soc. 124 (2002) 12108.
[27] Q. Lu, F. Gao, S. Komarneni, J. Am. Chem. Soc. 126 (2004) 54.
[28] X.Y. Chen, X.F. Zhang, C.W. Shi, X.L. Li, Y.T. Qian, Solid State Commun. 134 (2005) 613.
[29] C. Barglik-Chory, C. Remenyi, H. Strohm, G. Muller, J. Phys. Chem. B 108 (2004) 7637.
[30] B. Zhang, X.C. Ye, W. Dai, W.Y. Hou, Y. Xie, Chem-Eur. J. 12 (2006) 2337.
[31] B. Zhang, X.C. Ye, W. Hou, Y. Zhao, Y. Xie, J. Phys. Chem. B 110 (2006) 8978.
[32] H. Tong, Y.J. Zhu, L.X. Yang, L. Li, L. Zhang, J. Chang, L.Q. An, S.W. Wang, J. Phys. Chem. C 111 (2007) 3893.
[33] B. Halliwell, J.M.C. Gutteridge, Free Radicals in Biology and Medicine, Oxford University Press, 1999.
[34] R.A. Spurr, H. Myers, Anal. Chem. 29 (1957) 760.
[35] C.S. Gopinath, S.G. Hegde, A.V. Ramaswamy, S. Mahapatra, Mater. Res. Bull. 37 (2002) 1323.
[36] E. Papirer, R. Lacroix, J.B. Donnet, G. Nanse, P. Fioux, Carbon 33 (1995) 63.
[37] L. Zang, R.V. Koka, Mater. Chem. Phys. 57 (1998) 23.
[38] X. Chen, C. Burda, J. Phys. Chem. B 108 (2004) 15446.
[39] Y. Cong, J.L. Zhang, F. Chen, M. Anpo, J. Phys. Chem. C 111 (2007) 6976.
[40] H.X. Li, X.Y. Zhang, Y.N. Huo, J. Zhu, Environ. Sci. Technol. 41 (2007) 4410.
[41] T. Umebayashi, T. Yamaki, S. Tanaka, K. Asai, Chem. Lett. 32 (2003) 330.
[42] M. Sathish, B. Viswanathan, R.P. Viswanath, C.S. Gopinath, Chem. Mater. 17 (2005) 6349.
[43] L.K. Randeniya, A. Bendavid, P.J. Martin, E.W. Preston, J. Phys. Chem. C 111 (2007) 18334.
[44] N.C. Saha, H.G. Tompkins, J. Appl. Phys. 72 (1992) 3072.
[45] E. Gyorgy, A. Perez del Pino, P. Serra, J.L. Morenza, Surf. Coat. Technol. 173 (2003) 265.
[46] K.S.W. Sing, D.H. Everett, R.A.W. Haul, L. Moscou, R.A. Pierotti, J. Rouquerol, T. Siemieniewska, Pure Appl. Chem. 57 (1985) 603.
[47] D.C. Hurum, A.G. Agrios, K.A. Gray, T. Rajh, M.C. Thurnauer, J. Phys. Chem. B 107 (2003) 4545.
[48] J.W. Tang, H.D. Quan, J.H. Ye, Chem. Mater. 19 (2007) 116.
[49] H. Yamashita, M. Honda, M. Harada, Y. Ichihashi, M. Anpo, T. Hirao, N. Itoh, N. Iwamoto, J. Phys. Chem. B 102 (1998) 10707.
[50] A. Sclafani, J.M. Herrmann, J. Phys. Chem. 100 (1996) 13655.
[51] M. Andersson, L. Österlund, S. Ljungström, A. Palmqvist, J. Phys. Chem. B 106 (2002) 10674.
[52] M.C. Yan, F. Chen, J.L. Zhang, M. Anpo, J. Phys. Chem. B 109 (2005) 8673.
[53] B. Ohtani, K. Iwai, H. Kominami, T. Matsuura, Y. Kera, S. Nishimoto, Chem. Phys. Lett. 242 (1995) 315.
[54] Y. Cong, J.L. Zhang, F. Chen, M. Anpo, D.N. He, J. Phys. Chem. C 111 (2007) 10618.
[55] Y.Z. Li, N.H. Lee, D.S. Hwang, J.S. Song, E.G. Lee, S.J. Kim, Langmuir 20 (2004) 10838.
[56] K. Yanagisawa, J. Ovenstone, J. Phys. Chem. B 103 (1999) 7781.